Large Elastic, Plastic, and Creep Deflections of Curved Beams and Axisymmetric Shells

JAMES A. STRICKLIN,* PAO-TAN HSU,† AND THEODORE H. H. PIAN‡
Massachusetts Institute of Technology, Cambridge, Mass.

A numerical method is presented for analyzing large deflections of curved beams and large axisymmetric deflections of shells of revolution. The governing equations that are in finite-difference form are solved by a Newton-Raphson iteration procedure. The plastic stress-strain relations are determined by assuming three independent slip planes that are the planes of maximum shear stresses. The stress-strain relation along each slip plane is assumed to be linearly strain hardening. This plasticity model gives piecewise linear plasticity relations with determinate coefficients. For snap buckling problems, the so-called upper critical load is determined by introducing an artificial spring opposite to the applied load. The true load is then the difference between the applied load and the reaction of the spring. The important mathematical consequence of introducing the spring is to yield a single valued load-deflection curve, thus allowing the critical loads to be determined. The method is applied to several problems including low arches, circular rings, shallow and deep spherical shells under elastic-plastic deformations, and a shallow arch under creep deformation.

Nomenclature

A, B, C = stress-strain coefficients [Eqs. (16) and (17)]
$\bar{A}$ = area per unit width of sheet or flange [Eq. (50)]
E, E_1, E_p = slope of tensile stress-strain curve (Fig. 5)
F = force per unit area [Eq. (1)]
G_p = slope of plastic shear stress-strain curve (Fig. 5)
h = distance from midsurface to sheet or flange [Eq. (50)]
H = stress resultant in vertical direction [Eq. (43)]
K = spring constant [Eq. (44)]
L = number of finite-difference stations through thickness
M = stress couple and number of finite-difference stations for concentrated load [Eq. (51)]
N = stress resultant and number of finite-difference stations along midsurface
P = force per unit area [Eq. (2)]
Q = shear resultant (Figs. 1 and 10)
r = radius of curvature (Figs. 1 and 10)
r_1 = $X_0/\sin\phi_0$ = radius of curvature in circumferential direction
S = meridional distance (Fig. 3)
ΔS = finite-difference increment (Fig. 8)
t = thickness of shell or beam
T = time [Eq. (52)]
W = weighting factor for numerical integration [Eqs. (34–37)]
X = radial distance from axis of symmetry to midsurface (Fig. 1)
$\bar{X}$ = X at base of shell
Y = vertical distance from base to midsurface (Fig. 1)
Z = distance perpendicular to midsurface (Fig. 1)
α, β = coefficients for specifying boundary conditions [Eqs. (42 and 43)]
γ^p = plastic shear strain (Fig. 5)
δ^* = deflection [Eq. (44)]
ϵ = axial strain
θ = circumferential angle (Fig. 1)
λ = local distribution parameter [Eq. (44)] and shell parameter [Eq. (53)]
ν = Poisson's ratio
σ = normal stress
σ_0 = tensile yield stress (Fig. 5)
τ = shear stress
τ_0 = shear yield stress (Fig. 5)
ϕ = slope of midsurface (Fig. 1)
Λ = load distribution parameter [Eq. (44)]

Subscripts

j = integer for solution number
l = arbitrary thickness finite-difference station (Fig. 8)
m = value at midsurface
n = arbitrary midsurface finite-difference station (Fig. 8)
o = undeformed surface
p = plastic
z = direction normal to midsurface
θ = circumferential direction
ϕ = meridional direction

Superscripts

c = creep
e = elastic
p = plastic
t = thermal

Presented as Preprint 64-75 at the AIAA Aerospace Sciences Meeting, New York, January 20–22, 1964; revision received May 28, 1964. This research work was supported by the Office of Scientific Research, U. S. Air Force, under the Grants OSR-62-239 and OSR-347-63. The authors acknowledge the assistance of Evelyn Mack, who did the major programing, and the Massachusetts Institute of Technology Computation Center for the use of their facilities.

* Research Assistant, Department of Aeronautics and Astronautics; now Assistant Professor, Georgia Institute of Technology, Atlanta, Ga. Member AIAA.

† Senior Research Engineer, Aeroelastic and Structures Research Laboratory. Member AIAA.

‡ Associate Professor of Aeronautics and Astronautics. Associate Fellow Member AIAA.

Introduction

A METHOD has been developed[1] for predicting the response and permanent plastic deformation of curved beams and shells of revolution under dynamic loading conditions. That method, which employs a timewise step-by-step numerical analysis, is not applicable to static problems. The present paper is aimed at the static problems.

The present investigation also considers the buckling of shallow arches and shells under lateral loadings. The elastic buckling of shallow arches has been treated by Marguerre,[2] Fung and Kaplan,[3] and Hoff and Bruce.[4] The creep buckling of shallow arches has been considered by Pian and Chow.[5,6] Buckling of shallow spherical shells under uniform pressure has been treated by many authors.[7–15]

The main objective of the present investigation is to develop a general procedure that is suitable to analyze large

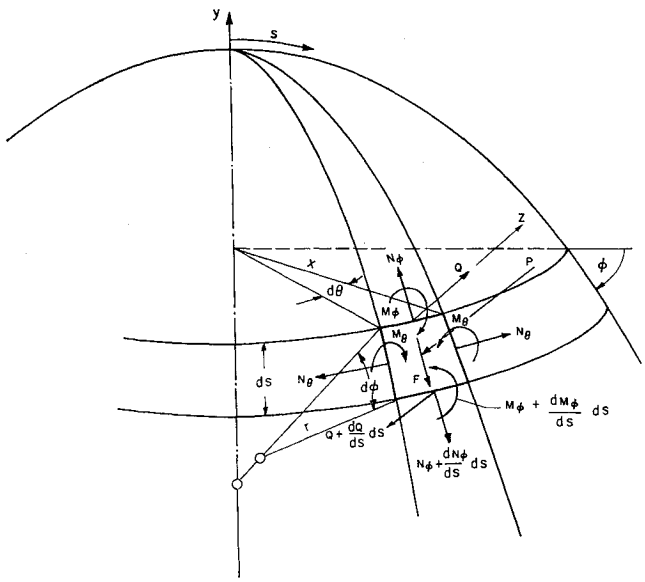

Fig. 1 Coordinate system and force equilibrium diagram.

plastic and creep deformations of shells of revolution. A number of examples are included to illustrate the versatility of the proposed method. The analysis of the large deflection behavior of curved beams is a much simpler problem, but it contains similar numerical procedures. A few examples on the static deflection of low arches and rings are also included as illustrations.

Equations for Axisymmetric Deflections of a Shell of Revolution

The analyses of curved beams and axisymmetric deflections of shells of revolution have many common features. For this reason, the governing equations, the finite difference representation, and the method of solution are discussed in detail for the shell, and only a brief discussion is made for the beam.

Assumptions

The assumptions for the analyses are:

1) Strains are negligible compared to 1.0.

2) Everywhere along the shell the ratio between the thickness and the radius of curvature in the deformed state is negligible compared to 1.0.

3) The material particles that lie on a normal to the midsurface of the undeformed shell lie on a normal to the deformed midsurface.

4) The deflections of the shell of revolution are axisymmetric.

5) Stresses normal to the midsurface of the structure are negligible.

6) The stress-strain curve, obtained from a tensile test, may be represented by straight line segments.

Equations of Equilibrium

The conditions of equilibrium of an element cut from a shell by two adjacent meridian planes and two sections perpendicular to the meridian (Fig. 1) can be written from standard text such as Timoshenko and Woinowsky-Krieger.[16] For the present purpose, however, the shell coordinates are referred to the deformed shell instead of the undeformed shell. Also, the nomenclature used here is somewhat different from that in Ref. 16. For example, the curvature $1/r$ is replaced by $d\phi/dS$, where ϕ is the slope of the meridian, and S is the distance along the meridian.

The equations of force equilibrium and of moment equilibrium are

$$d(N_\phi X)/dS - N_\theta \cos\phi - QXd\phi/dS + FX = 0 \quad (1)$$

$$N_\phi X d\phi/dS + N_\theta \sin\phi + d(QX)/dS + PX = 0 \quad (2)$$

$$d(M_\phi X)/dS - M_\theta \cos\phi - QX = 0 \quad (3)$$

where Q, N_ϕ, N_θ, M_ϕ, and M_θ are the stress resultants and stress couples defined by

$$Q = \int_{-t/2}^{t/2} \tau_{\phi z} dZ \quad (4)$$

$$N_\phi = \int_{-t/2}^{t/2} \sigma_\phi dZ \quad (5)$$

$$M_\phi = -\int_{-t/2}^{t/2} \sigma_\phi Z dZ \quad (6)$$

$$N_\theta = \int_{-t/2}^{t/2} \sigma_\theta dZ \quad (7)$$

$$M_\theta = -\int_{-t/2}^{t/2} \sigma_\theta Z dZ \quad (8)$$

and F and P are the applied forces per unit area along the directions tangent and normal to the midsurface of the deformed shell. X is the distance from a point on the meridian to the axis of symmetry.

Geometry of Deformed Surface

From Fig. 2 it can be seen that the equations that describe the deformed surface are

$$dX/dS = \cos\phi \quad (9)$$

$$dY/dS = -\sin\phi \quad (10)$$

$$d\phi/dS = 1/r \quad (11)$$

$$dS = (1 + \epsilon_{\phi m})dS_0 \quad (12)$$

where $\epsilon_{\phi m}$ is the midsurface strain in the direction of N_ϕ. dS_0 is a differential element of length of the midsurface of the undeformed body.

Compatibility Equation

The compatibility equation is an expression of the circumferential strain in terms of a horizontal displacement of a ring of material. To derive this equation, consider the undeformed and deformed shell as shown in Fig. 3.

Let a given point be specified by the undeformed midsurface radius X_0 and the distance Z perpendicular to the midsurface. This point will occupy the position X, Z in the de-

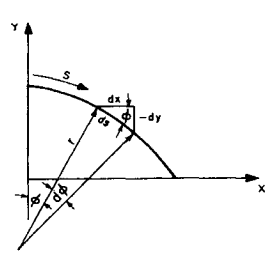

Fig. 2 Geometry of deformed surface.

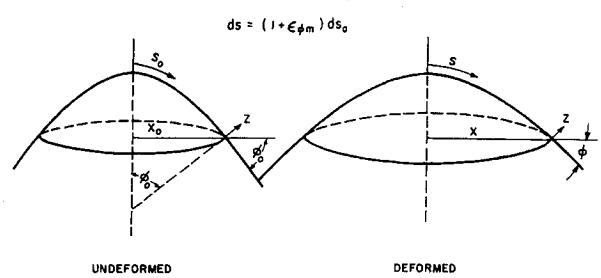

Fig. 3 Deformed and undeformed midsurfaces of a shell.

formed body. The circumferential strain is, by definition, given by the change in the circumferential length divided by the original length, i.e.,

$$\epsilon_\theta = \frac{2\pi[X + Z\sin\phi - (X_0 + Z\sin\phi_0)]}{2\pi(X_0 + Z\sin\phi_0)}$$

$$= \frac{1}{1 + Z/r_1}\left[\frac{(X - X_0)}{X_0} + Z\left(\frac{\sin\phi}{X_0} - \frac{1}{r_1}\right)\right]$$

where $1/r_1 = (\sin\phi_0)/X_0$.

For thin shells where Z/r_1 is small, the foregoing expression reduces to

$$\epsilon_\theta = (X - X_0)/X_0 + Z(\sin\phi/X_0 - 1/r_1) \qquad (13)$$

The first term $(X - X_0)/X_0$ is the circumferential strain $\epsilon_{\theta m}$ of the midsurface and can be expressed in terms of $\epsilon_{\phi m}$ as follows:

$$\frac{(X - X_0)}{X_0} = \epsilon_{\theta m} = \frac{1}{X_0}\int_0^{S_0}[\cos\phi(1 + \epsilon_{\phi m}) - \cos\phi_0]dS_0 =$$

$$\frac{-2}{X_0}\int_0^{S_0}\sin\frac{\phi + \phi_0}{2}\sin\frac{\phi - \phi_0}{2}\,dS_0 + \frac{1}{X_0}\int_0^{S_0}\cos\phi\;\epsilon_{\phi m}dS_0 \qquad (14)$$

In the foregoing derivation, the trigonometric identity

$$\cos\phi - \cos\phi_0 = -2\sin\frac{\phi + \phi_0}{2}\sin\frac{\phi - \phi_0}{2}$$

has been used to prevent excessive roundoff error in the numerical computation.

Strain-Curvature Relations

The strain-curvature relation is a geometrical equation based on the assumption that elements normal to the midsurface remain normal to the deformed surface. As may be found in Ref. 17, this equation is

$$\epsilon_\phi = \epsilon_{\phi m} + Z(d\phi/dS - 1/r_0) \qquad (15)$$

Here again the curvature is replaced by $d\phi/dS$.

Stress-Strain Relations

The general expressions for the linear stress-strain relations may be written as

$$\epsilon_\phi = A_\phi + B_\phi\sigma_\phi + C_\phi\sigma_\theta + \epsilon_\phi{}^t + \epsilon_\phi{}^c \qquad (16)$$

$$\epsilon_\theta = A_\theta + B_\theta\sigma_\phi + C_\theta\sigma_\theta + \epsilon_\theta{}^t + \epsilon_\theta{}^c \qquad (17)$$

where the superscripts t and c stand for thermal and creep, respectively. The coefficients A, B, and C are functions of the stresses σ_ϕ and σ_θ and are dependent on the strain hardening rule employed in the analysis. The derivation of these stress-strain coefficients is given in the following section.

Stress-Strain Coefficients

The current development in the theory of plasticity has not reached a stage such that a precise statement of the plastic stress-strain relations can be obtained. Thus, in practice, the choice as to which relation to use in a given situation is somewhat governed by mathematical convenience.

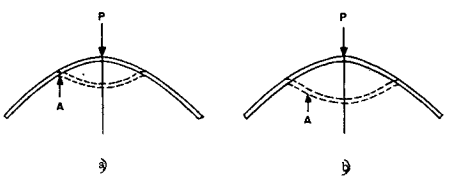

Fig. 4 Typical deflection shapes for different loads.

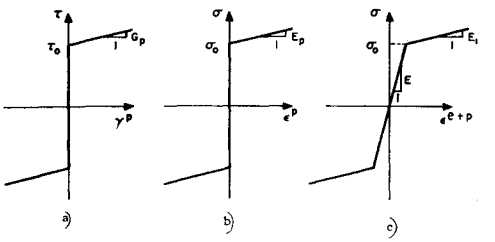

Fig. 5 Stress-strain curves.

Prior to the derivation of suitable stress-strain coefficients, a remark should first be made of the possible loading paths in the stress space. Test results on a spherical shell under a gradually increasing concentrated load have indicated a rather sharp bend at the transition region between the buckled portion and the unbuckled portion (point A in Fig. 4a). This means that the inside surface of the shell at point A will have a negative value in ϵ_ϕ. However, when the shell deforms further, the transition region moves outward, and the strain ϵ_ϕ at the inside surface at point A may be reversed and reach a large positive value (Fig. 4b). This shows that an element of the material may first yield in compression, then unload, and finally reload in tension until another part of the yield surface is reached.

The stress-strain relations used to represent this rather complicated behavior are derived from two basic assumptions:

1) All the plastic strain is due to slipping along three independent slip planes§ along each of which the shear is a maximum. For the present problem of axisymmetric deformations of shells of revolution, the stresses σ_z, $\tau_{\theta z}$, and $\tau_{\phi\theta}$ are zero. For thin shells, the magnitude of the transverse shear stress $\tau_{\phi z}$ is of a smaller order of magnitude in comparison to the normal stresses σ_ϕ and σ_θ. It is thus justified to neglect $\tau_{\phi z}$ in the stress-strain relations. It is seen that ϕ, θ, and Z are the principal stress directions, and the magnitudes of the maximum shear stresses are $\sigma_\phi/2$, $\sigma_\theta/2$, and $(\sigma_\phi - \sigma_\theta)/2$. They are acting in the planes that bisect two of the principal directions. These planes are denoted by (ϕ, z), (θ, z), and (ϕ, θ), respectively.

2) The plastic strain contributed by each set of slip planes may be represented by a finite number of straight lines and is the same for positive and negative shear stress. For simplicity in the example calculations in this paper, only one linear strain hardening relation is employed as shown in Fig. 5a. It is seen that the plastic shear strain γ^p is given by

$$\gamma^p = (\tau - (\pm)\tau_0)/G_p \qquad (18)$$

where the sign is chosen to be the same as the sign of τ.

Consider now the implications of this slip plane model. First, it is observed that yielding based on the maximum shear stress gives, by definition, the Tresca yield condition.

The correspondence between various segments on the yield surface and slip planes is defined as follows: segments AB and DE correspond to planes (ϕ, Z); BC and EF to (θ, Z); and CD and FA to (ϕ, θ).

Next, the plastic normal strains $\epsilon_\phi{}^p$ and $\epsilon_\theta{}^p$, resulting from slip, are determined by Mohr's circle for strain. For the different yielding regions, the plastic normal strains are given as follows:

If

$$|\sigma_\phi| > \sigma_0 \qquad |\sigma_\theta| < \sigma_0 \qquad |\sigma_\phi - \sigma_\theta| < \sigma_0$$

$$\epsilon_\phi{}^p = \tfrac{1}{4}[\sigma_\phi - (\pm)\sigma_0]/G_p = -\epsilon_z{}^p$$

$$\epsilon_\theta{}^p = 0 \qquad (19)$$

§ Bernard Budiansky has pointed out that a similar plasticity model has been developed by J. H. Palm.[18] The only difference is that Palm represents the unaxial stress-strain curve by an exponential function, whereas this analysis uses two straight lines for the unaxial stress-strain curve.

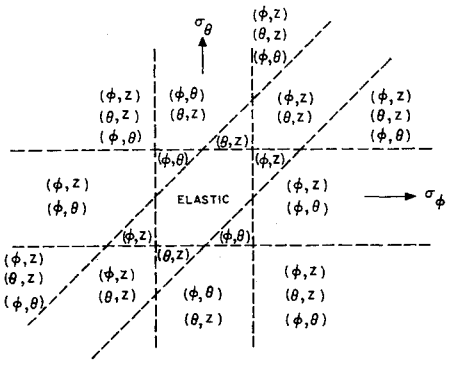

Fig. 6 Slip-plane contributions for different regions in stress space.

If

$$|\sigma_\phi| < \sigma_0 \qquad |\sigma_\theta| > \sigma_0 \qquad |\sigma_\phi - \sigma_\theta| < \sigma_0$$
$$\epsilon_\theta{}^p = \tfrac{1}{4}[\sigma_\theta - (\pm)\sigma_0]/G_p = -\epsilon_z{}^p \tag{20}$$
$$\epsilon_\phi{}^p = 0$$

If

$$|\sigma_\phi| < \sigma_0 \qquad |\sigma_\theta| < \sigma_0 \qquad |\sigma_\phi - \sigma_\theta| > \sigma_0$$
$$\epsilon_\phi{}^p = \tfrac{1}{4}[\sigma_\phi - \sigma_\theta - (\pm)\sigma_0]/G_p = -\epsilon_\theta{}^p \tag{21}$$
$$\epsilon_z{}^p = 0$$

where the sign is chosen, respectively, to be the same as the sign of σ_ϕ, σ_θ, and $\sigma_\phi - \sigma_\theta$.

With these basic relations, the total plastic strain can be computed for any loading by simply adding the plastic strain that is contributed by each slip plane. For example, in simple tension where $\sigma_\theta = 0$ and $\sigma_\phi > \sigma_0$, the planes (ϕ, Z) and (ϕ, θ) are activated. Thus, the total plastic strain is obtained by combining Eqs. (19) and (21), i.e.,

$$\epsilon_\phi{}^p = \tfrac{1}{2}(\sigma_\phi - \sigma_0)/G_p \tag{22}$$
$$\epsilon_\theta{}^p = -\tfrac{1}{4}(\sigma_\phi - \sigma_0)/G_p \tag{23}$$

The first of these relations also can be used to determine the relation between the constants from a simple tension test specimen and those of the slip plane model. From Fig. 5b it is seen that the plastic strain from a simple tension test specimen is given by

$$\epsilon_\phi{}^p = (\sigma_\phi - \sigma_0)/E_p \tag{24}$$

Equating the different expressions for the plastic strain $\epsilon_\phi{}^p$, one obtains

$$\frac{1}{2G_p} = \frac{1}{E_p} = \frac{1}{E_1} - \frac{1}{E} \tag{25}$$

When a material is under only loading conditions, the slip planes that contribute to the total strain in various regions of stress space are summarized in Fig. 6.

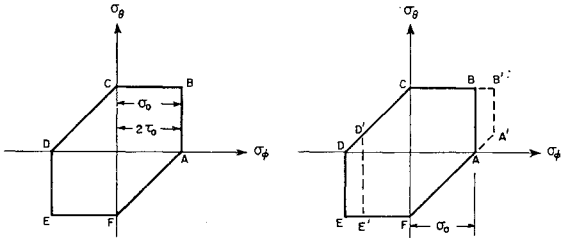

Fig. 7 Tresca yield boundary and subsequent yield surface for strain hardening.

Subsequent Yield Surfaces

From the assumed shear stress-strain diagram, it is seen that the distance between lines that represent positive and negative yielding is a constant. From this, it follows that the corresponding segments of the yield surface must maintain a constant distance $2\sigma_0$. For example, if the line segment AB in Fig. 7 moves a distance $\sigma_\phi - \sigma_0$ to the right, the segment DE must move the same distance to the right. The new yield surface is now given by $A'B'CD'E'F$.

Computational Procedure

The stress-strain coefficients can be computed by independently adding the contribution of each set of slip planes. Consider, for example, the (ϕ, Z) planes. When $|\sigma_\phi| < \sigma_0$, the (ϕ, Z) planes contribute nothing to the plastic strains; but when $|\sigma_\phi| > \sigma_0$, these planes are activated and the new coefficients, according to Eqs. (19) and (25), should be

$$A_\phi = A_\phi{}' - (\pm)\frac{\sigma_0}{2}\left(\frac{1}{E_1} - \frac{1}{E}\right)$$
$$B_\phi = B_\phi{}' + \frac{1}{2}\left(\frac{1}{E_1} - \frac{1}{E}\right) \tag{26}$$
$$C_\phi = C_\phi{}' \qquad A_\theta = A_\theta{}' \qquad B_\theta = B_\theta{}' \qquad C_\theta = C_\theta{}'$$

where the primed coefficients include the effects of both the elastic strains and the plastic strains which are contributed by the other two slip planes.

If unloading occurs after yielding, the coefficients become

$$A_\phi = A_\phi{}'' + \frac{\sigma_{\phi u}}{2}\left(\frac{1}{E_1} - \frac{1}{E}\right)$$
$$B_\phi = B_\phi{}'' - \frac{1}{2}\left(\frac{1}{E_1} - \frac{1}{E}\right) \tag{27}$$
$$C_\phi = C_\phi{}'' \qquad A_\theta = A_\theta{}'' \qquad B_\theta = B_\theta{}'' \qquad C_\theta = C_\theta{}''$$

where $\sigma_{\phi u}$ is the stress value at which unloading starts. The double primed coefficients are the values of the coefficients which existed prior to unloading. The net contribution of the (ϕ, Z) planes after yielding and unloading is to add to A_ϕ the expression $\frac{1}{2}(\sigma_{\phi u} - (\pm)\sigma_0)[(1/E_1) - (1/E)]$ and to leave the other coefficients unchanged.

After yielding occurs in the opposite direction, $|\sigma_{\phi u} - \sigma_\phi| > 2\sigma_0$, the coefficients become

$$A_\phi = A_\phi{}''' + (\pm)(2\sigma_0 - |\sigma_{\phi u}|)\frac{1}{2}\left(\frac{1}{E_1} - \frac{1}{E}\right)$$
$$B_\phi = B_\phi{}''' + \frac{1}{2}\left(\frac{1}{E_1} - \frac{1}{E}\right) \tag{28}$$
$$C_\phi = C_\phi{}''' \qquad A_\theta = A_\theta{}''' \qquad B_\theta = B_\theta{}''' \qquad C_\theta = C_\theta{}'''$$

where the sign is chosen to be the same as the sign of $\sigma_{\phi u}$.

The total contribution of the (ϕ, Z) planes after Eqs. (28) are employed is the same as would have been obtained if the opposite sign had been chosen in Eqs. (26). Hence, all future contribution of the (ϕ, Z) planes are covered by Eqs. (27) and (28).

The contributions from the (θ, Z) and (ϕ, θ) planes are treated the same way, except the coefficients are changed in accordance with Eqs. (20) and (21). It is seen that, by using this computational procedure, the coefficients for any stress history and stress values can be obtained without writing down explicitly the stress-strain relations for each possible loading path.

Numerical Representation

For the numerical representation, it is assumed that there are N equally spaced finite-difference stations along the midplane of the shell and L equally spaced finite-difference sta-

tions through the thickness. n and l represent arbitrary finite-difference stations along the length and through the thickness of the shell (Fig. 8).

The numerical representation consists of writing the differential equations and integrals in terms of the values of the variables at the finite-difference stations. The strain-curvature relations and stress-strain relations, being algebraic equations, are satisfied at all finite-difference stations. After combining Eqs. (13) and (15) with (16) and (17), the following equations are obtained in finite-difference form:

$$(N_\phi X)_{n+1} = (N_\phi X)_n + [N_\theta \cos\phi + QX(d\phi/dS) - XF]_n \Delta S_0 \tag{29}$$

$$(QX)_{n+1} = (QX)_n - [N_\phi X(d\phi/dS) + N_\theta \sin\phi + PX]_n \Delta S_0 \tag{30}$$

$$(M_\phi X)_{n+1} = (M_\phi X)_n + (M_\theta \cos\phi + QX)_n \Delta S_0 \tag{31}$$

$$\epsilon_{\theta mn} + Z_{ln}[(\sin\phi/X_0) - (1/r_1)]_n = A_{\theta ln} + B_{\theta ln}\sigma_{\phi ln} + C_{\theta ln}\sigma_{\theta ln} + \epsilon_{\theta ln}{}^t + \epsilon_{\theta ln}{}^c \tag{32}$$

$$\epsilon_{\phi mn} + Z_{ln}[(d\phi/dS) - (1/r_0)]_n = A_{\phi ln} + B_{\phi ln}\sigma_{\phi ln} + C_{\phi ln}\sigma_{\theta ln} + \epsilon_{\phi ln}{}^t + \epsilon_{\phi ln}{}^c \tag{33}$$

$$N_{\theta n} = \Delta Z_n \sum_{l=1}^{L} \sigma_{\theta ln} W_l \tag{34}$$

$$M_{\theta n} = -\Delta Z_n \sum_{l=1}^{L} \sigma_{\theta ln} W_l Z_{ln} \tag{35}$$

$$N_{\phi n} = \Delta Z_n \sum_{l=1}^{L} \sigma_{\phi ln} W_l \tag{36}$$

$$M_{\phi n} = -\Delta Z_n \sum_{l=1}^{L} \sigma_{\phi ln} Z_{ln} W_l \tag{37}$$

$$(X - X_0)_n = (X - X_0)_{n-2} - \frac{2\Delta S_0}{3}\left[\left(\sin\frac{\phi + \phi_0}{2}\sin\frac{\phi - \phi_0}{2}\right)_{n-2} + 4\left(\sin\frac{\phi + \phi_0}{2}\sin\frac{\phi - \phi_0}{2}\right)_{n-1} + \left(\sin\frac{\phi + \phi_0}{2}\sin\frac{\phi - \phi_0}{2}\right)_n\right] + \frac{\Delta S_0}{3} \times [(\epsilon_{\phi m}\cos\phi)_{n-2} + 4(\epsilon_{\phi m}\cos\phi)_{n-1} + (\epsilon_{\phi m}\cos\phi)_n] \tag{38}$$

$$\epsilon_{\theta mn} = (X - X_0)_n / X_{0n} \tag{39}$$

$$Y_n = Y_{n-2} - (\Delta S_0/3)\{[\sin\phi(1 + \epsilon_{\phi m})]_{n-2} + 4[\sin\phi(1 + \epsilon_{\phi m})]_{n-1} + [\sin\phi(1 + \epsilon_{\phi m})]_n\} \tag{40}$$

$$\phi_{n+1} = \phi_{n-1} + 2\Delta S_0 (d\phi/dS)_n \tag{41}$$

where ΔS, ΔZ, Z_l, X, and Y are shown in Fig. 8, and W is a weighting factor for numerical integration through the thickness of the shell. The finite-difference representations consist of forward differences for the equations of equilibrium, Simpson integrations for X, Y, and $X - X_0$, and central differences for $d\phi/dS$.

Boundary Conditions

The boundary conditions for the axisymmetric deflection of a shell of revolution are specified at the apex and at the base. At the apex $\phi = 0$, $X = 0$, $M_\phi = M_\theta$, $N_\phi = N_\theta$. At the base, several possible boundary conditions can be represented by the expressions

$$\alpha_1 \phi_N + \alpha_2 M_{\phi N} + \alpha_3 = 0 \tag{42}$$

$$\beta_1 \epsilon_{\theta mN} + \beta_2 H_N = 0 \tag{43}$$

where H_N is the vertical stress resultant at the base and α_1, α_2, α_3, β_1, and β_2 depend on the desired boundary conditions. For example, if the base is clamped, $\alpha_1 = 1.0$, $\alpha_2 = 0$, $\alpha_3 = -\phi^*$, $\beta_1 = 1.0$, and $\beta_2 = 0$, where ϕ^* is the slope of the shell at the base.

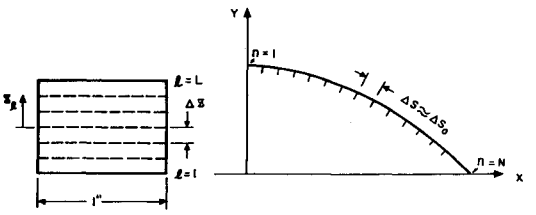

Fig. 8 Finite-difference model of a beam or a shell.

Solution of the Equations

The solution of the finite-difference equations is accomplished by using a Newton-Raphson iteration procedure. It will be shown that, for a given loading, the stress resultant and stress couple at the apex determine completely the behavior of the shell of revolution. The Newton-Raphson method is used to determine the correct values of these variables which satisfy the boundary conditions prescribed at the base.

Since the loading path is important for plasticity considerations, the loads must be increased in increments. In the case of creep problems, the time T is the independent variable. During each time increment, the external loads P_n and F_n, the thermal strains, $\epsilon_\phi{}^t$ and $\epsilon_\theta{}^t$, and the creep strains $\epsilon_\phi{}^c$ and $\epsilon_\theta{}^c$ vary. For this discussion, the term "condition j" is used to indicate the values of P_n, F_n, $\epsilon_{\phi ln}{}^t$, $\epsilon_{\theta ln}{}^t$, $\epsilon_{\phi ln}{}^c$, and $\epsilon_{\theta ln}{}^c$ at the end of the jth increment, and a subscript j will be included whenever a clarification of the equations is needed. It is assumed that the solutions have been obtained for conditions 1, 2, 3, . . . j-2, j-1, and the solution is desired for condition j.

Trial values for $N_{\phi 1j}$ and $M_{\phi 1j}$ are obtained by a linear extrapolation from solutions at conditions j-2 and j-1. Also, the stress-strain coefficients are made consistent with the stresses obtained by a linear extrapolation from their values at conditions j-2 and j-1. When unloading occurs, the stress value at condition j-1 is assumed to be the one where unloading starts. The accuracy of this extrapolation procedure is controlled by allowing only a limited number of the stress-strain coefficients to change when going from condition j-1 to condition j.

Consider that at "condition j," the geometric parameters, stress-strain coefficients, and boundary conditions are prescribed, and the trial values of $N_{\phi 1}$ and $M_{\phi 1}$ have been obtained. The solution can then be carried out to the nth finite-difference station; hence the values of $N_{\phi n}$, $M_{\phi n}$, and ϕ_n can be obtained. Then the calculation procedure is:

1) The $2L + 5$ equations given by Eqs. (32–39) are used to determine $M_{\theta n}$, $N_{\theta n}$, $\epsilon_{\phi mn}$, $\epsilon_{\theta mn}$, $(d\phi/dS)_n$, $\sigma_{\theta ln}$, and $\sigma_{\phi ln}$. For this solution, $\sigma_{\theta ln}$, $\sigma_{\phi ln}$, and $\epsilon_{\theta mn}$ are eliminated by using Eqs. (32, 33, and 39), which leaves four linear equations to be solved for $\epsilon_{\phi mn}$, $(d\phi/dS)_n$, $N_{\theta n}$, and $M_{\theta n}$.

2) Equations. (29–31 and 41) give $M_{\phi n+1}$, $N_{\phi n+1}$, Q_{n+1}, and ϕ_{n+1}.

3) Calculation steps 1 and 2 are repeated until $n = N$ and the boundary conditions are checked.

4) If the boundary conditions are not satisfied, the partial derivatives of the boundary condition variables are determined as forward differences and used in the Newton-Raphson procedure to obtain new trial values for $M_{\phi 1}$ and $N_{\phi 1}$.

5) Using the new values of $M_{\phi 1}$ and $N_{\phi 1}$, the four previous steps are repeated until the boundary conditions are satisfied to within the desired tolerances. The calculation can then be proceeded to condition $j + 1$.

For problems that involve a peak load in the load deflection reuve, the procedure just outlined will encounter difficulty

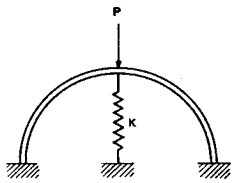

Fig. 9 Elastic foundation for determining critical load.

when the applied load approaches the critical load. At the critical load, the determinant of the partial derivatives, used in the Newton-Raphson procedure, will become singular. For the large class of problems of proportional loading, this difficulty can be avoided by considering the shell to be supported by an elastic foundation such that the net loads P_n and F_n are reduced to

$$P_{nj} = \lambda_n \bar{P}_j(1 - K\delta^*/\bar{P}_j)$$
$$F_{nj} = \Lambda_n \bar{P}_j(1 - K\delta^*/\bar{P}_j) \tag{44}$$

where $\bar{P}_j$ is the reference loading parameter, K the spring constant, λ_n and Λ_n the parameters that specify the load distribution, and δ^* the deflection of a suitably chosen station.

For the present work, δ^* was chosen as the deflection of the apex when a concentrated load was applied (Fig. 9) and was chosen as the maximum deflection when a uniform load was applied. The maximum deflection was chosen since the deflection of a particular station does not necessarily increase monotonically under uniform loading. Other alternatives for the parameter δ^* are the change in volume, slope of a particular station, etc.

The solution now consists of specifying values of $\bar{P}_j$ and determining the resulting P_n and F_n. The only modification to the method of solution is to include the parameter δ^* as another unknown in the Newton-Raphson procedure.

In this study, an additional check was added to require the stress-strain coefficients to be consistent with the actual stresses instead of being consistent with extrapolated values for the stresses. This is accomplished by comparing the stresses and coefficients after the first step in the computing cycle to see if they are consistent. If the stresses are outside the range of applicability of the coefficients, the coefficients are made consistent with the computed stress, and the computing cycle is then repeated. By using this additional feature, the possibility of using incorrect coefficients is avoided, but it is believed that this additional complication is not needed if the loading increments are small.

Curved Beams

The curved beam analysis is carried out by using essentially the method that was just described. The equations representing the curved beam replace those representing the shell, but the iterational method for solving the equations is the same. However, the unsymmetrical behavior of a curved beam can be analyzed by this method if the shear resultant Q is included as another variable in the Newton-Raphson procedure. Then, the stress resultants and stress couple would be assumed at one boundary and the solution carried to the other boundary.

The equations of equilibrium, which correspond to those for the shell of revolution, are (see Fig. 10)

$$dN_\phi/dS - Qd\phi/dS + F = 0 \tag{45}$$
$$N_\phi d\phi/dS + dQ/dS + P = 0 \tag{46}$$
$$dM_\phi/dS - Q = 0 \tag{47}$$

The corresponding finite-difference equations can be obtained in a similar manner.

The stress-strain relation for linear strain hardening is given by the simple expression

$$\epsilon_\phi = A_\phi + B_\phi\sigma_\phi + \epsilon_\phi{}^t + \epsilon_\phi{}^c \tag{48}$$

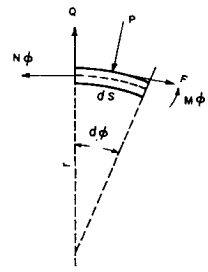

Fig. 10 Differential element of a beam.

As shown in Fig. 5c, the stress-strain coefficients are determined through the relation

$$\epsilon_\phi{}^p = (\sigma_\phi - (\pm)\sigma_0)[(1/E_1) - (1/E)] \tag{49}$$

Applications

The numerical procedure discussed previously has been used to solve several different types of shell and beam problems. For these solutions, the thickness of the shell is represented by two sheets, and the thickness of the beam is represented by three flanges of equal area. The cross-sectional area and separation distance of the sheets or flanges were determined by requiring the mathematical model and actual specimen to have the same flexural rigidity and either the same area or the same ultimate moment per unit width. These conditions are expressed, respectively, by the equations

Shell	Beam
$2\bar{A}h^2 = t^3/12$	$2\bar{A}h^2 = t^3/12$
$2\bar{A} = t$	$3\bar{A} = t$
$2\bar{A}h = t^2/4$	$2\bar{A}h = t^2/4$

(50)

where $\bar{A}$ is the area per unit width of the sheet or flange, and h is the distance from the midsurface to the sheet or flange.

Since it is impossible both physically and mathematically to apply a point load to a shell of revolution, the load is assumed to be distributed over a finite area in accordance with the following equations:

$$P_n = P \quad n < M$$
$$P_n = P/2 \quad n = M \tag{51}$$
$$P_n = 0 \quad n > M$$

where M is a specified number and P is the loading parameter.

Elastic Deflection of a Spherical Cap under a Concentrated Load

Figure 11 shows the experimental and theoretical load-deflection curves for a spherical cap whose slope at the base is approximately 17°. The experimental results[19] were obtained by applying the load through a rubber pad of diameter $\frac{3}{4}$ in. In the theoretical analysis, N, the number of finite-difference

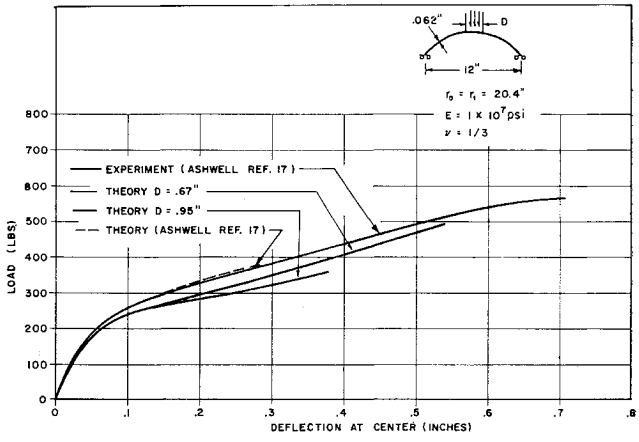

Fig. 11 Load-deflection curve for elastic spherical cap.

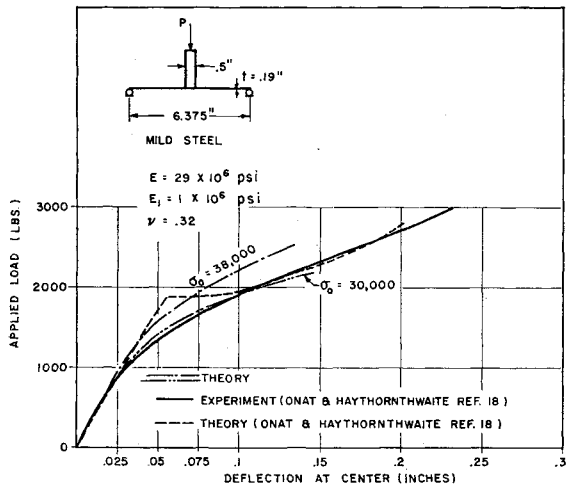

Fig. 12 Load-deflection curve for a flat plate.

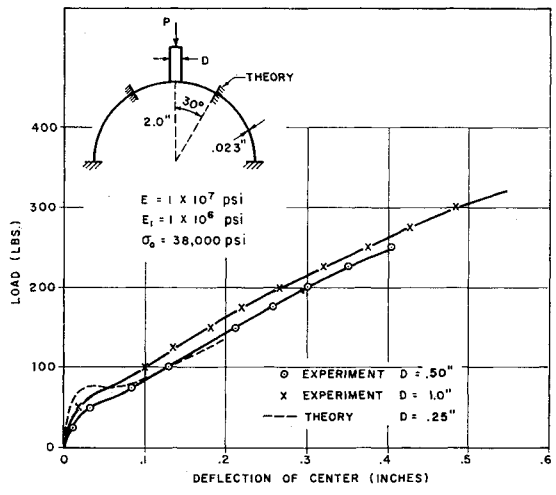

Fig. 13 Theoretical and experimental load-deflection curves for a spherical cap.

stations, is 91, $\bar{A} = t/2, h = t/2\,(3)^{1/2}$, and the base is assumed to be simply supported.

It is observed that the theoretical curve lies below experimental values. Archer[12] also obtained results for shallow shells that lie below the experimental values. Using linear shallow shell equations, Ashwell[19] obtained results that agree exceedingly well with experimental results, but he states that the agreement is probably fortuitous. Furthermore, his experimental results indicate that the yield stress of the material was exceeded during the experiment. The yield stress for the material was not given; hence, the position on the load deflection curve where the stress exceeds the yield stress is not known.

Elastic-Plastic Deflection of a Circular Plate

Figure 12 shows the experimental and theoretical results for a circular steel plate under a concentrated load. In the experiment,[20] a centrally placed punch of ½-in. diam was used to apply the load. In the theoretical solution, $N = 76$, $2\,\bar{A}h^2 = t^3/12$, $2\,\bar{A}h = t^2/4$, and the base is simply supported.

The theoretical curves were obtained for a yield stress of 30,000 and 38,000 psi, whereas the average yield stress of the mild steel from which the test specimen was made is 32,000 psi. Also shown in this figure is Onats and Haythornthwaite's theoretical results that were obtained by linearly adding the elastic deflections to those obtained from a rigid, perfectly plastic analysis.

Elastic-Plastic Deflection of a Spherical Cap under a Concentrated Load

Results for the elastic-plastic deflection of a spherical cap are shown in Fig. 13. For the experiments, hemispherical shells of 4 in. in diameter and 0.023 in. thick were prepared from 6061-O aluminum alloy by hydroforming, spinning, and chemical milling. The thickness variations were as large as ±10%. The specimens were heat-treated to a Rockwell hardness of 74–80, resulting in a measured compressive yield stress of 36,000 psi for 0.2% offset and an ultimate tensile stress of 42,500 psi. The base of the shell was clamped by placing the shell in liquid cerrobend and allowing the cerrobend to solidify. The concentrated load was applied through 0.5- and 1.0-in. steel balls.

Instead of analyzing the hemispherical shell, the theoretical analysis was conducted on a spherical cap whose slope ϕ^* at the undeformed base is 30°. This simplifying assumption is justified since only membrane forces exist in most of the unbuckled part of the shell. In the theoretical analysis, $N = 76$, $2\,\bar{A}h^2 = t^3/12$, $2\,\bar{A} = t$, and the base is assumed to be clamped.

The results show good qualitative agreement after the shell buckles and would probably agree better at the buckling load if the same distribution of the concentrated load had been used. A slight change in the slope of the experimental load-deflection curve occurs at a deflection of approximately 0.2 in. when the axisymmetric deflection shape degenerates to a multisided one.

Elastic-Plastic Behavior of a Semi-Ring under a Point Load

Figure 14 shows the experimental and theoretical load deflection curve for a semi-ring under a point load. For the experiments,[21] circular rings of 1.97-in. radius, 0.0625-in. thickness, and 1-in. width were machined from 6061-T6 aluminum tubing. The thickness was uniform along the circumference of the ring. The rings were mounted in a steel base and clamped at 90° from the apex by a wedge. The load was applied at the apex, and the deflection of the apex increased monotonically.

The mathematical model had the same moment of inertia and ultimate moment as the test specimen. The agreement between theory and experiment is considered to be good.

Elastic-Creep Deflection of a Shallow Arch

The ability of the method to solve creep problems is illustrated on a shallow arch as shown in Fig. 15. The creep strains were computed from the equation

$$\epsilon_{\phi lnj}{}^{c} = \epsilon_{\phi lnj-1}{}^{c} + \left(\frac{\sigma_{\phi lnj-1}}{50{,}000}\right)^{3} \Delta T \qquad (52)$$

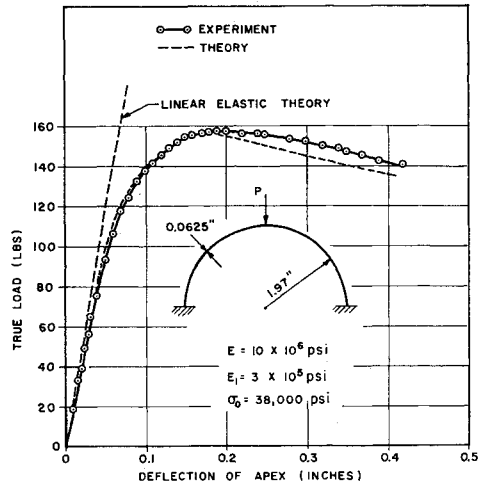

Fig. 14 Theoretical and experimental load deflection curves for a clamped ring.

The nondimensional time $\Delta T = 0.35$ was used as the time interval between condition j-1 and j. The critical buckling time T_{cr} was 5.071. The geometry of the arch that was analyzed is the same as that of the specimen which was used in the experimental investigations conducted by Gjelsvik and Bodner.[22] The results were not compared, because the creep law for the aluminum alloy used by Gjelsvik and Bodner is not known.

Discussions and Conclusions

Some other results, not presented in this paper, are the buckling of shallow elastic shells under uniform pressure. In these studies, solutions were obtained for several values of the shell parameter λ, which is defined by

$$\lambda^2 = 2[3(1 - \nu^2)]^{1/2}\bar{X}^2/r_0 t \qquad (53)$$

Although the shallow shell assumptions were not used in this analysis, the computed buckling pressures are essentially the same as those obtained through the shallow shell equations. For example, for the shell parameter λ equal to 20.0, the

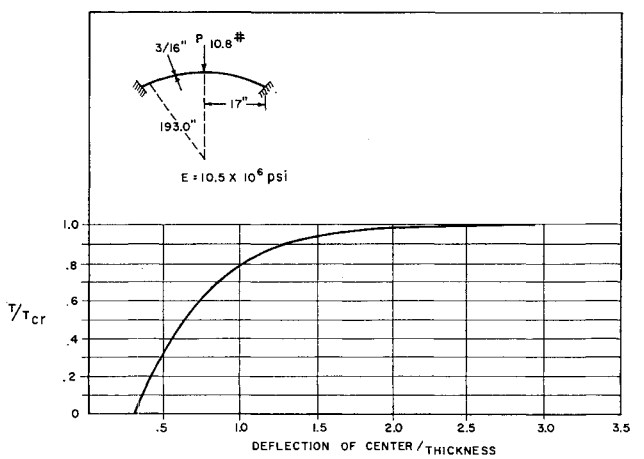

Fig. 15 Creep deflection at center of shallow arch.

buckling pressure was computed to be 0.982 of the classical buckling pressure. For this case, Archer[12] obtained a ratio of 0.987. These results, however, are of little practical value since, as the investigation of Huang[14] has shown, asymmetric buckling occurs when the value of the shallow shell parameter λ is greater than 6.0. The solution for $\lambda = 20$ does, however, demonstrate that the Newton-Raphson procedure, as presented here, will converge for complex deflection shapes.

The convergence of the solution with the number of finite-difference stations along the midsurface was partially checked through ring and shallow shell studies. It was found that the use of 76 and 91 finite-difference stations for the ring gave essentially the same answer, and the use of 76 and 101 finite-difference stations for the shallow shell yielded results that differ by a small amount. Additional checks for the convergence of the solution with the number of finite-difference stations along the midsurface are needed; but, more important, the number of finite-difference stations through the thickness must be increased if plasticity and creep strains are present.

In general, it is concluded that this method can be used to study the elastic, plastic, thermal, and/or creep behavior of beams and shells of revolution which deflect axisymmetrically.

References

[1] Witmer, E. A., Balmer, H. A., Leech, J. W., and Pian, T. H. H., "Large dynamic deformations of beams, rings, plates, and shells," AIAA J. **1**, 1848–1857 (1963).

[2] Marguerre, K., "On the application of the energy method to stability problems," NACA TM 1138 (1947).

[3] Fung, Y. C. and Kaplan, A., "Buckling of low arches and curved beams of small curvature," NACA TN 2840 (1952).

[4] Hoff, N. J. and Bruce, V. G., "Dynamic analysis of the buckling of laterally loaded flat arches," J. Math. Phys. **32**, 276–288 (1953).

[5] Pian, T. H. H., "Creep buckling of curved beam under lateral loading," *Proceedings of the U.S. National Congress of Applied Mechanics* (American Society of Mechanical Engineers, New York, 1958), pp. 649–654.

[6] Pian, T. H. H. and Chow, C. Y., "Further studies of creep buckling of curved beam under lateral loading," TR 25-28, Aeroelastic and Structures Research Lab., Massachusetts Institute of Technology (December 1958).

[7] Von Karman, T. and Tsien, H. S., "The buckling of spherical shells by external pressure," J. Aeronaut. Sci. **7**, 43–50 (1939).

[8] Kaplan, A. and Fung, Y. C., "A non-linear theory of bending and buckling on thin elastic shallow spherical shells," NACA TN 3212 (1954).

[9] Budiansky, B., "Buckling of clamped shallow spherical shells," *Proceedings of I.U.T.A.M. Symposium on the Theory of Thin Elastic Shells* (North-Holland Publishing Co., Amsterdam, 1960), pp. 64–94.

[10] Weinitschke, H. J., "On the stability problem for shallow spherical shells," J. Math. Phys. **38**, 209–231 (1959).

[11] Thurston, G. A., "A numerical solution of the nonlinear equations for axisymmetric bending of shallow spherical shells," J. Appl. Mech. **28**, 557–562 (1961).

[12] Archer, R. R., "On the numerical solution of the nonlinear equations for shells of revolution," J. Math. Phys. **41**, 165–178 (1962).

[13] "Collected papers on instability of shell structures," NASA TN D-1510 (1962).

[14] Huang, N. C., "Unsymmetrical buckling of shallow spherical shells," AIAA J. **1**, 945 (1963).

[15] Roth, R. S., "Plastic buckling of thin shallow spherical shells," TR 13, Div. of Engineering and Applied Physics, Harvard Univ. (May 1962).

[16] Timoshenko, S. and Woinowsky-Krieger, S., *Theory of Plates and Shells* (McGraw-Hill Book Co., Inc., New York, 1959), p. 533.

[17] Timoshenko, S. and Gere, J. M., *Theory of Elastic Stability* (McGraw-Hill Book Co., Inc., New York, 1961), p. 440.

[18] Palm, J. H., "Stress-strain relations for uniform monotonic deformation under triaxial loading," Appl. Sci. Res. **A2**, 54–92 (1951).

[19] Ashwell, D. G., "On the large deflection of a spherical shell with an inward point load," *Proceedings of I.U.T.A.M. Symposium on the Theory of Thin Elastic Shells* (North-Holland Publishing Co., Amsterdam, 1960), pp. 43–63.

[20] Onat, E. T. and Haythornthwaite, R. M., "Load carrying capacity of circular plates at large deflections," J. Appl. Mech. **23**, 49–55 (1956).

[21] Witmer, E. A., Hermann, W., Leech, J. W., and Pian, T. H. H., "Responses of plates and shells to intense external loads of short duration," Wright Air Development Div. TR 60-433, Massachusetts Institute of Technology Aeroelastic and Structures Research Lab. (April 1960).

[22] Gjelsvik, A. and Bodner, S. R., "An investigation of the energy criterion in snap buckling problems with applications to clamped arches," Brown Univ., TR 28 (February 1962).

[23] Naghdi, P. M., "Stress-strain relations in plasticity and thermoplasticity," *Plasticity, Proceedings of the Second Symposium on Naval Structures Mechanics* (Pergamon Press, New York, 1960).

[24] Stricklin, J. A., "Large elastic, plastic, and creep deflections of curved beams and axisymmetric shells," Ph.D. Thesis, Massachusetts Institute of Technology (January 1964).